Polarization Alignment for Cellular-based Mobile Aerial Communication

Yongjae Yoo, Seungmin Choi, Jeongyeup Paek, Saewoong Bahk

***Abstract*—Cellular communication in the sky will become increasingly important in the near future with the rise of airborne services such as drone taxis. While polarization has traditionally been a secondary concern in terrestrial communication due to multipath and reflections, the dominance of line-of-sight paths in aerial environment makes polarization alignment critical. This study is the first to conduct both experimental and mathematical analyses of polarization alignment to estimate the unknown polarization characteristics of commercial cellular base stations from the aerial device's perspective. We perform real measurements to evaluate these estimations, verifying the base station's practical polarization profile and validating our model. Using this model, we then propose *PACMAN*, a method that identifies the optimal polarization for each drone position, thereby enhancing alignment and maximizing throughput. By combining polarization prediction with antenna steering, *PACMAN* improves signal-to-noise-ratio and throughput by 20.7% on average (up to 67% in peak scenarios), offering a novel approach to optimizing cellular-based aerial communication systems.**

***Index Terms*—Unmanned Aerial Vehicle, Polarization Alignment, Cellular Communication, Aerial Network**

I. Introduction

The global unmanned aerial vehicle (UAV) industry has experienced a compound annual growth rate of approximately 30% from 2015 to 2024, with projections indicating a significant acceleration in the coming years [1]. This growth is driving increased demand for drone technology across various sectors, including military [2], [3], agriculture [4], and urban air mobility [5]. A prominent characteristic of recent UAVs (a.k.a drones) is the demand for high throughput; e.g. vision-guided drones require transmission of high-resolution camera data. This trend is expected to intensify as the use of drones continues to expand.

Various technologies have been proposed for drone communication, but short-range wireless solutions like Wi-Fi are insufficient for these applications due to limited range and coverage [6]–[9]. To ensure seamless communication over long distances, cellular communication provide the most suitable option, offering extended coverage and stable connectivity required for aerial applications [10]–[14]. Then, the research problem is to maximize throughput of drones on commercial cellular networks while minimizing changes to existing infrastructure that are designed for terrestrial users.

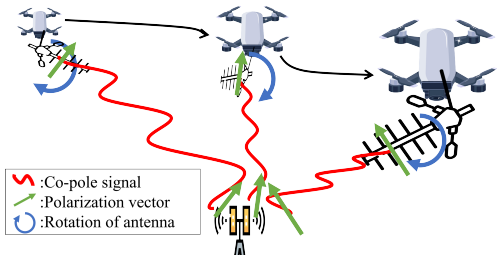

Fig. 1: Illustration of rotating antenna on drones for polarization alignment to a cellular base station

In this work, we explore the impact of polarization in UAV communication and demonstrate that aligning a drone's antenna polarization can unlock significant untapped throughput. For terrestrial users, polarization has not been a critical concern, as multipath effects in ground environments (especially indoors) tend to depolarize or mix signals, leading to similar performance regardless of received polarization [15]. However, the situation is different for drones due to the higher chance of maintaining a dominant line-of-sight (LoS) path. Through real-world drone measurements, we show that signal strength and throughput vary significantly with polarization in aerial communication, unlike for ground users (§II). These findings highlight the need for a method that dynamically aligns the drone's antenna angle during flight to maximize communication efficiency.

Literature review (§II-A) indicates that only a few studies have examined throughput in aerial network, and even fewer have investigated polarization in cellular-based UAV communication. Some prior work investigate antennas for aerial networks with consideration of polarization [16]; however, these studies lack solutions for run-time adaption. Moreover, most of these studies are simulation-based and lack real-world measurements, a significant limitation without evidence [11], [13], [14].

To the best of our knowledge, this study is the first to measure and model polarization and its impact on a drone against a commercial cellular network actively in use (§III). We conduct experiments by flying a real drone equipped with a LTE modem and a SIM card. The drone is outfitted with a

Y. Yoo, S. Choi, and S. Bahk are with the Department of Electrical and Computer Engineering and INMC, Seoul National University, Seoul, Republic of Korea (email: yjyoo@netlab.snu.ac.kr, seungminchoi22@snu.ac.kr, sbahk@snu.ac.kr). J. Paek is with the Department of Computer Science and Engineering, Chung-Ang University, Seoul, Republic of Korea (email: jpaek@cau.ac.kr). S. Bahk and J. Paek are the corresponding authors.

This work was supported by the Institute of Information & communications Technology Planning & Evaluation (IITP) under the ITRC(Information Technology Research Center) support program (IITP-2024-2021-0-02048), Next-generation Cloud-native Cellular Network Leadership Program(IITP-2025-RS-2024-00418784) funded by the Korea government (MSIT), and also by the National Research Foundation of Korea (NRF) grant funded by the Korea government (MSIT) (No. RS-2024-00359450).

motor and a control board to enable active rotation of the antenna, allowing us to measure the signal characteristics while adjusting the antenna's orientation and model the polarization profile of the base station. These unique aspects differentiate our work from previous studies and establish its novelty.

Based on the model derived from this data, we propose *PACMAN* (§IV), a method that consists of two stages: One is to explore the unknown polarization of the base station by rotating the antenna at a couple sampling points, and the other is to calculate the UAV polarization vector at arbitrary positions to achieve our ultimate goal: maximize throughput by taking advantage of the polarization effectively.

The contributions of this paper are as follows:

- We demonstrate that, unlike terrestrial devices where polarization has minimal impact, polarization can significantly affect performance in cellular-based aerial communication.
- We develop a mathematical model to predict how the base station's polarization will appear to a receiving antenna on a drone, and validate this model using real-world data.
- Based on the model, we propose *PACMAN*, a method that dynamically adjusts the drone's antenna polarization to align with that of the base station with minimal exploration, ensuring optimal fit at any arbitrary position within the base station's coverage area.
- We design and assemble a comprehensive experimental prototype to measure the observed base station polarization and evaluate *PACMAN* in real-world scenarios.

The remainder of the paper is organized as follows: In §II, we review existing research to differentiate the novelty of our work, and provide background on the characteristics of cellular base station's polarization. In §III, we present a mathematical model to determine the unknown polarization of antennas, and use this model to design *PACMAN* in §IV. We evaluate *PACMAN* in §V, and discuss its limitations and directions for future work in §VI. Finally, we summarize the work in §VII.

II. Preliminary

In this section, we review existing research on polarization and antenna steering in UAV applications. We then examine the impact of polarization alignment on drone throughput. Finally, we summarize key insights from our findings.

A. Related Work

Polarization. There has been substantial research on antenna polarization, with many studies focusing on polarization diversity and methodologies to enhance it [17]–[20]. However, majority of these works are limited to antenna design and theoretical modeling, with most evaluations conducted in controlled simulations which often fail to account for the complexities of practical deployment in aerial environments [21]–[25]. Few studies have addressed polarization effects under dynamic conditions or on real commercial networks. In contrast, our work differs by focusing on in-situ measurements from antennas deployed in the field, providing practical insights into polarization performance in cellular-based aerial communication under dynamic scenarios.

Antenna Steering in UAV. Some studies suggest that antenna alignment is essential for improving drone performance. Pokorny *et al.* [26] propose a UAV-based backhaul link equipped with a directional antenna and an autonomous steering system to provide stable connectivity in remote and emergency scenarios. Wang *et al.* [27] propose a multi-tier UAV communication network model that addresses the challenges of random beam misalignment, providing an analytical framework for outage probability under imperfect alignment conditions. Dabiri *et al.* [28] conduct a downlink interference analysis for UAV-based mmWave fronthaul networks, considering realistic channel parameters such as UAV vibrations and random small cell base station distribution. Kim *et al.* [29] explores long-range air-to-ground communication systems using a monopulse tracking method, focusing on maintaining reliable tracking performance despite dynamic UAV maneuvers.

While the concept of antenna rotation for drones partially aligns with our approach, previous studies have not addressed polarization alignment. Our study is the first to tackle this challenge in real-world scenarios, making a novel and distinctive contribution to UAV communication systems.

Polarization in UAV. Several studies have explored signal polarization in the context of drones. Wen *et al.* [30] propose a 3D positioning method using a bi-static polarized MIMO radar, leveraging AoA and AoD measurements to determine UAV locations without requiring coordination between base stations and UAVs. However, this differs from our work, as the drone primarily acts as a reflector rather than actively transmitting and receiving signals. Badi *et al.* [31] experimentally analyze how the drone body affects received power and cross-polarization discrimination (XPD) in drone-to-drone communication, showing that relative positioning significantly impacts power variations. While this study provides useful insights, it focuses on drone-to-drone communication rather than interactions with a commercial base station and does not propose a real-time polarization alignment solution.

Similarly, Cheng *et al.* [7] conducted field measurements but their analysis was confined to Wi-Fi links which operate differently from the cellular networks central to our study. On the other hand, Asadpour *et al.* [8] suggested the use of circular polarization to mitigate mismatch, but this remains a conceptual proposal without experimental validation nor a focus on dynamic alignment for linear polarization.

Ge *et al.* [32] propose a 3D geometrical-based polarized model for UAV-correlated MIMO channels, analyzing the impact of UAV tilt rotation, cross-polarization, and antenna spacing on channel capacity. Their study provides valuable insights for UAV communication network design and is the most similar to our approach. However, it is also limited to simulations based on existing datasets and does not includemechanisms for polarization optimization or run-time adjustments.

B. Motivation

Previous studies have explored polarization to a limited extent. This is because for typical cellular users, the environment is predominantly non-line-of-sight (NLoS) where the effects

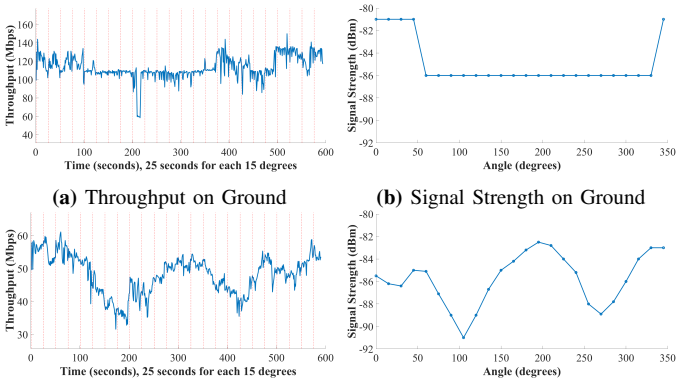

(a) Throughput on Ground **(b)** Signal Strength on Ground

(c) Throughput on Air **(d)** Signal Strength on Air

Fig. 2: Ground vs. Air comparison on the influence of polarization on throughput and signal strength.

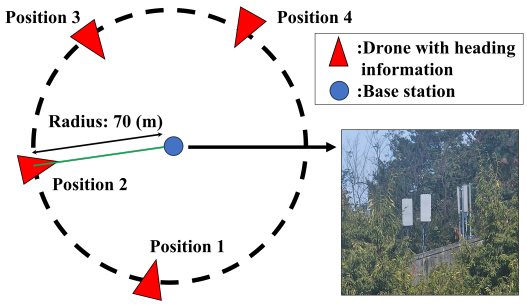

Fig. 3: Exploratory Experiment Location

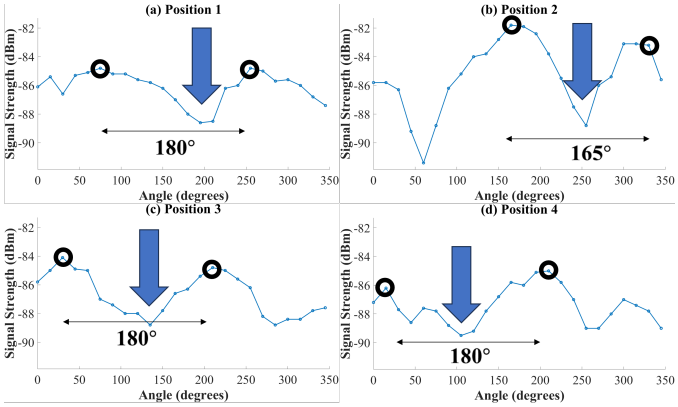

Fig. 4: Signal strengths by polarization with peaks (black circles) and holes (blue arrows) at each position

of multipath reduces the impact of polarization. As a result, despite base stations transmit with *fixed slant polarization* and users are oblivious of that, polarization mismatch has minimal impact to terrestrial users. However, the situation is different in aerial environments because, in the sky, a direct line-of-sight (LoS) path exists with higher probability and is dominant. Polarization (mis-)alignment does impact performance and thus becomes critically important. Through the following experiments, we demonstrate how ground users and aerial users differ in terms of their response to polarization.

We conduct measurements both in the air and on the ground. For this purpose, we attach a commercial antenna to a drone and rotate the antenna using a motor while measuring signal strength and throughput. The setup consists of a Raspberry Pi 4 board connected to an LTE modem, with throughput evaluated using iPerf 3 application. Using a motor, we are able to accurately adjust the angle in 15-degree increments (smallest granularity in our setup), from 0 to 360 degrees (24 distinct angles). We then measured the throughput for 25 seconds at each angle. Further details of the experimental setup can be found in §V-A. For comparison, we perform the same measurement on the ground at the same 2D location using identical equipment and setup, with the only difference being the altitude (0 vs. 50 meters above ground).

Fig. 2 summarizes our measurement results. Fig. 2a plots the throughput when a ground user is oriented towards the base station at each specific polarization angles (25 seconds for each 15 degrees). It shows that ground users experience relatively stable throughput regardless of the polarization angle. This outcome can be explained by the signal strength in Fig. 2b, measured as Reference Signal Received Power (RSRP). The graph indicates no significant variation in signal strength across different angles. In contrast, Fig. 2c and Fig. 2d plot the throughput and signal strength when an aerial device is oriented towards the base station at specific polarization angles. Unlike the ground results, they reveal that certain angles result in stronger signal strength for aerial users. Consistent with this trend, it is possible for aerial users to achieve higher throughput when the antenna is aligned at specific angles. These findings motivate us to find the best antenna angle for drone's throughput.

C. Exploratory Experiment

Several articles indicate that commercial base stations use *fixed slant polarization* [33], [34]. Through exploratory experiments, we confirm that base stations indeed exhibit a specific fixed polarization[1].

Similar to our previous experiments, we rotate the antenna on the drone 360 degrees using a motor while the antenna's azimuth is aligned toward the base station. The antenna is rotated about the normal vector of its plane, ensuring that the polarization angle is adjusted as the antenna rotates. We again use RSRP to verify the alignment with the base station's polarization, consistent with previous measurements in Figs. 2b and 2d. Note that the measurements in this paper are for downlink transmissions. Although throughput is the preferred metric for network optimization, it can vary unpredictably in commercial networks due to reasons other than signal quality such as resource allocation by the service provider or varying user loads, thus making consistent reproducible testing challenging. Additionally, while Received Signal Strength Indicator (RSSI) could be used, it is susceptible to noise and interference from other signals, leading to significant deviations. In contrast, RSRP, which uses a fixed channel, is less affected by such issues, making it a suitable

[1]It is possible that the dominant signal component is a reflection off the ground instead of line-of-sight direct path. Nevertheless, it does not change the fact that a dominant signal with polarization is observed by the drone.

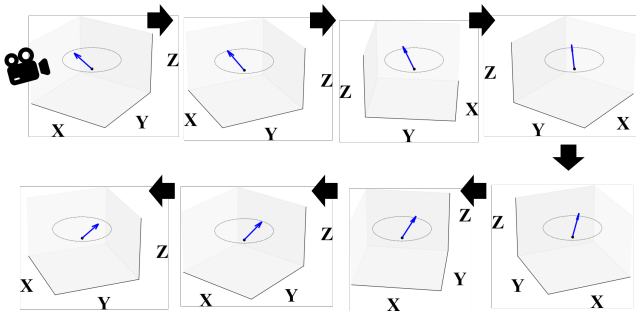

Fig. 5: Watching a fixed vector from different viewpoints

and representative metric for accurately reflecting polarization alignment. Our expectations are as follows: If the base station generates a fixed polarization, then

1) signal from the base station will have two RSRP peaks during a 360-degree rotation, indicating *co-polarization alignment*;
2) similarly, there will be two points where the signal is weakest (holes) during a 360-degree rotation, indicating *cross-polarization alignment*;
3) the intervals showing co-polarization (peak intervals) and cross-polarization (hole intervals) will be separated by 180 degrees, with holes located between peaks.

To verify these hypotheses, we rotate the antenna in 15-degree increments, holding each position for 10 samples and calculating the average signal strength (RSRP) at each angle. Fig. 4 plots the RSRP data obtained from the base station at each explored positions in Fig. 3. It shows that, regardless of location, our results align with the hypothesis (double peak/hole shape), confirming that the observed signal strength data matches our expectations.

D. Insights

Our preliminary exploration reveals the following insights: commercial cellular base stations use fixed polarization, aerial devices are affected significantly by polarization (unlike ground users), and aligning the antenna's polarization can result in substantial throughput gains. These findings highlight the critical role of polarization in aerial networks and underscore the need for a method to determine the optimal antenna orientation to match polarization in such settings.

Motivated by these observations, we design *PACMAN*, a method that enables the drone to dynamically explore and identify the base station's polarization while in flight. Using this information, *PACMAN* can then compute the optimal antenna angle to achieve the best alignment at any unexplored drone positions.

This is made possible by the following intuition: the antenna angle yielding the highest signal strength shifts depending on the drone's current position (e.g., positions 1, 2, 3, and 4 in Fig. 3). This indicates that the perceived polarization angle of the base station varies based on the location of the receiving antenna. As illustrated in Fig. 5, a fixed vector in three-dimensional space appears at different angles depending on the observer's position. Similarly, the polarization of the signal emitted by the base station's antenna appears differently depending on the drone's position and perspective. This insight reinforces the concept that effective polarization alignment requires adapting to the unique viewing angle of the drone in real-time. In the following section, we further explore this concept using a mathematical approach, employing vector projection techniques to quantify and adjust for these positional changes in perceived polarization.

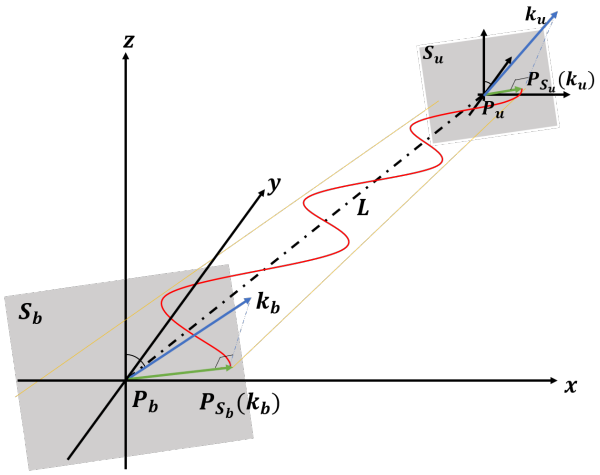

Fig. 6: Diagram of base station signal's polarization

III. Modeling Polarization for UAV

In this section, we present how a drone in actual flight can identify the polarization angle of the base station and, in turn, calculate the optimal antenna angle at each drone position to maximize signal strength.

A. Mathematical concept of aligning two polarization vectors.

We devise a model to identify the unknown polarization of a base station. Note that the meaning of polarization vector k and $-k$ are consistent. Therefore, in the following discussion, we assume that k is constrained such that its z-coordinate satisfies $z \geq 0$. Although instantaneous attitude jitter may occur in practice, we define k as the dominant orientation of the antenna in this model assuming that the impact of high-frequency fluctuations is averaged out in the received signal power.

As illustrated in Fig. 6, assume that the base station is located at position P_b and the drone at P_u in a 3-D xyz space. Without loss of generality, let the base station be at the origin $O(0, 0, 0)$. Then, we define a line L connecting the central axis of the base station antenna and the central axis of the drone antenna[2]. Using L as the normal vector, we define two planes: S_b, which passes through the base station P_b and has L as its normal vector, and S_u, which passes through the drone position P_u with L as its normal.

[2]In our polarization alignment methodology, we assume that the position of the base station is known and the antenna mounted on the drone can be freely adjusted to any orientation. This approach has been devised in numerous studies [26]–[29].

Since the signal emitted from the base station meets the far-field conditions, we assume that it is received by the drone as a plane wave.[3] The planes S_b and S_u represent the surfaces along which this plane wave propagates between the base station and the drone.

We define the vector of the plane wave generated by the base station antenna (*polarization vector*) as k_b. Considering the relationship between the UAV and the base station, k_b alone holds limited significance. Instead, we need to relate the vector with its LOS channel direction. This can be effectively obtained using *projection* techniques. The projected vector of k_b onto S_b, denoted as $P_{S_b}(k_b)$, represents a vector on S_b where the actual wave propagates along the line L connecting the two antennas with $P_{S_b}(k_b)$ oriented perpendicular to L.

To identify the angle at which the signal strength is maximized (commonly referred to as the *co-polarization angle*), we rotate the angle of the drone-mounted antenna (γ) through 360 degrees (more detailed illustration in Fig. 7). γ rotates within the antenna plane, which is defined with n as its normal vector, and is measured relative to the basis vector n_2 within the plane. However, a challenge arises because the rotational alignment of the drone's antenna does not necessarily guarantee alignment with the plane wave's polarization angle. This discrepancy is due to the fact that the normal vector of the drone's antenna plane is not identical to S_u. In other words, the direction vector of L is not parallel with the normal vector of the drone's antenna plane.

Consequently, knowing the base station's polarization vector k_b does not directly allow us to determine the exact angle at which the drone antenna should rotate to to achieve co-polarization alignment. Instead, it becomes crucial to understand how the rotation of the antenna aligns within the propagation planes S_b and S_u where the plane wave travels.

To address this problem, we project the polarization vector k_u of the drone's antenna onto the plane S_u, yielding $P_{S_u}(k_u)$. Only at this point can we assert that the angle between the projected polarization vector of the drone's antenna ($P_{S_u}(k_u)$) and the projected polarization vector of the plane wave from the base station ($P_{S_b}(k_b)$) represent the true angular relationship between the two polarizations. When these vectors align, we achieve the optimal signal strength, indicating *co-polarization*. Definitions of notations in this paper are listed in Table I.

TABLE I: Notation and Parameter Definitions

Symbol	Definition
P_b	Base station position (origin)
P_{u_j}	jth UAV (drone) position
L	Line between base station and UAV antenna centers
L_j	Line between base station and jth UAV antenna centers
S_b	Plane through P_b, normal vector L
S_{u_j}	Plane through P_{u_j}, normal vector L_j
S_{b,u_j}	Plane through P_b, normal vector L_j
k_b	Base station polarization vector
k_{u_j}	jth UAV antenna polarization vector
$P_{S_i}(k_j)$	Projection of k_j onto plane S_i
θ_j	Azimuth angle of the polarization vector at position j
ϕ_j	Elevataion angle of polarization vector at position j
$\hat{\theta}_j$	Estimated azimuth angle of polarization vector at position j
$\hat{\phi}_j$	Estimated elevataion angle of polarization vector at position j
n	Antenna plane normal vector, defined as $n \cdot (0,0,1) \geq 0$
n_j	Basis vector for antenna plane ($j = 1, 2$)
α	Azimuth of the normal vector (n) of antenna plane
β	The heading of the antenna elevated about the z-axis.
γ	The polarization vector rotated within the antenna plane.

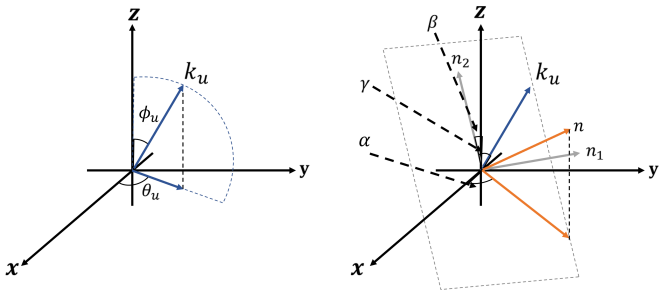

Fig. 7: Geometric representation of the polarization vector at the UAV. The antenna orientation is defined by three angles: the azimuth α (rotation around the Z-axis), the elevation β (tilt from the Z-axis), and the polarization angle γ (rotation within the antenna plane).

B. Two representations of polarization vector at the UAV.

k_u is a 3-D vector that the direction only matters. Thus, k_u can be represented using two angle parameters θ_u and ϕ_u (spherical coordinate with $r = 1$) as follows:

$$k_u(\theta_u, \phi_u) = \begin{pmatrix} \sin\theta_u \cos\phi_u \\ \sin\theta_u \sin\phi_u \\ \cos\theta_u \end{pmatrix} \tag{1}$$

Specifically, the antenna orientation is controlled by three parameters: (1) the *azimuth angle* α, defined as the angle of the normal vector projected onto the xy-plane relative to the x-axis; (2) the *elevation angle* β, defined as the angle between the normal vector and the z-axis; and (3) the *polarization angle* γ, which represents the rotation of the polarization vector within the antenna plane itself.

$$n_1 = \begin{pmatrix} -\sin\alpha \\ \cos\alpha \\ 0 \end{pmatrix}, \quad n_2 = \begin{pmatrix} -\sin\beta\cos\alpha \\ -\sin\beta\sin\alpha \\ \cos\beta \end{pmatrix} \tag{2}$$

n_1 and n_2 are the two basis for the antenna plane. Thus, polarization vector k_u can be represented as linear combination of the two vectors.

$$k_u = \sin\gamma \cdot n_1 + \cos\gamma \cdot n_2 \tag{3}$$

$$k_u(\alpha, \beta, \gamma) = \begin{pmatrix} -\sin\gamma\sin\alpha - \cos\gamma\sin\beta\cos\alpha \\ \sin\gamma\cos\alpha - \cos\gamma\sin\beta\sin\alpha \\ \cos\gamma\cos\beta \end{pmatrix} \tag{4}$$

Note that the polarization vector of the base station k_b is fixed, so there is no need to express it in terms of α, β or γ; using θ, ϕ notation is sufficient.

[3]This assumption is justified by the Fraunhofer distance criterion ($d \geq 2D^2/\lambda$). With $\lambda \approx 0.17$ m (1.8 GHz) and $D \approx 1.5$ m, the far-field region begins at ≈ 27 m. Our experiments at 50 m satisfy this. Furthermore, future Urban Air Mobility (UAM) applications operating at higher altitudes (e.g., 300–600 m) will even more strictly satisfy this plane wave condition.

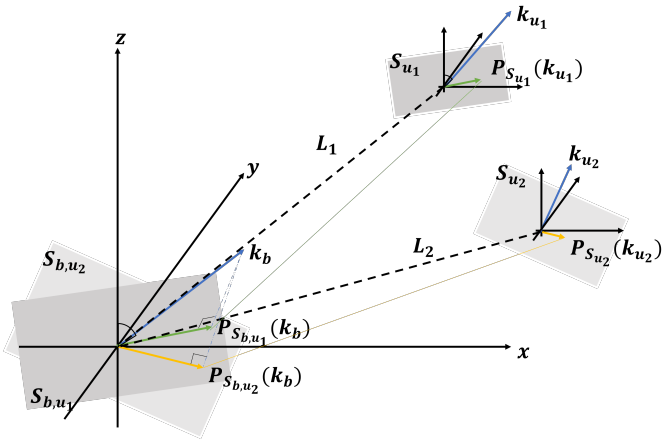

Fig. 8: Polarization of base station signal with two UAV positions

C. Finding the polarization vector of base station.

To determine the base station polarization vector k_b, two measurements are required at the minimum since k_b consists of two variable θ_b and ϕ_b. Additional measurements may be required to enhance the estimation accuracy. Thus, our goal is to estimate θ_b and ϕ_b via small number of observation samples.

From a single rotation at a fixed position, the only information obtained is the angle γ at which the signal strength is maximized (α and β are also known to us because they are controlled angles by UAV). With this information, we can identify only a vector $P_{S_b}(k_b)$ that lies on the plane S_b, which is parallel to S_u at the origin.

However, this information alone is insufficient to define a unique k_b vector as there are infinitely many vectors that, when projected onto S_b, result in $P_{S_b}(k_b)$. To ultimately resolve the polarization generated by the base station in a plane-wave channel, we derive the necessary formulations in a configuration illustrated in Fig. 8.

Let P_b to origin for convenience. At two distinct positions, $P_{u_1}(X_1, Y_1, Z_1)$ and $P_{u_2}(X_2, Y_2, Z_2)$, the drone rotates its antenna 360 degrees to find the polarization alignment. The lines connecting the drone to the base station at these positions are denoted as L_1 and L_2, respectively.

At P_{u_1}, let the antenna direction set to α_1 and β_1. If the best polarization angle is measured as γ_1, $k_{u_1}(\alpha_1, \beta_1, \gamma_1)$ is obtained. Similarly, $k_{u_2}(\alpha_2, \beta_2, \gamma_2)$ can be obtained at P_{u_2}.

By projecting the drone's antenna angle k_{u_1} onto plane S_{u_1} which has L_1 as its normal vector, $P_{S_{b,u_1}}(k_{u_1})$ is obtained. It is important to recall that result of $P_{S_{u_1}}(x)$ and $P_{S_{b,u_1}}(x)$ is exactly identical to each other for all 3-D vector x.

$$P_{S_{b,u_1}}(k_{u_1}) = P_{S_{u_1}}(k_{u_1}) = k_{u_1} - (k_{u_1} \cdot L_1)L_1 \tag{5}$$

The same approach can be applied to k_{u_2} measured at P_{u_2}.

$$P_{S_{b,u_2}}(k_{u_2}) = P_{S_{u_2}}(k_{u_2}) = k_{u_2} - (k_{u_2} \cdot L_2)L_2 \tag{6}$$

Similarly, for fitting the polarization vectors, projecting the base station's polarization vector k_b onto the planes $P_{S_{b,u_1}}$ and $P_{S_{b,u_2}}$ are necessary.

$$P_{S_{b,u_1}}(k_b) = k_b - (k_b \cdot L_1)L_1$$
$$P_{S_{b,u_2}}(k_b) = k_b - (k_b \cdot L_2)L_2$$

The base station's polarization vector $k_b(\theta_b, \phi_b)$ is uniquely determined by these projections. The criterion for matching the polarization vectors can be represented as follows:

$$\begin{aligned} P_{S_{b,u_1}}(k_b(\theta_b, \phi_b)) &= P_{S_{b,u_1}}(k_{u_1}) \\ P_{S_{b,u_2}}(k_b(\theta_b, \phi_b)) &= P_{S_{b,u_2}}(k_{u_2}) \end{aligned} \tag{7}$$

Since we already know all information in Eq. (7) except θ_b and ϕ_b, it is possible to obtain the closed form of $\hat{\theta}_b$ and $\hat{\phi}_b$.

D. Reconstruction of best antenna rotation angle UAV.

Finally, using the identified base station polarization $\hat{k}_b$ ($\hat{\theta}_b$, $\hat{\phi}_b$), it is possible to find the antenna polarization angle (or rotation angle) γ_i. Our goal is to determine γ_i at an arbitrary position $P_{u_i}(X_i, Y_i, Z_i)$, based on the given antenna settings α_i and β_i. We only consider the situation that P_{u_i} is connected to the base station at P_b (no handover occurred).

$$\hat{k}_b = \begin{pmatrix} \sin\hat{\theta}_b \cos\hat{\phi}_b \\ \sin\hat{\theta}_b \sin\hat{\phi}_b \\ \cos\hat{\theta}_b \end{pmatrix} \tag{8}$$

The vector obtained by projecting $\hat{k}_b$ onto the plane S_{b,u_i} should match with the vector obtained by projecting k_{u_i} onto the plane S_{b,u_i}.

$$P_{S_{b,u_i}}(\hat{k}_b) = P_{S_{b,u_i}}(k_{u_i}) \tag{9}$$

The left-hand side of Eq. (9) can be calculated as Eq. (10) (see next page). Since this is a constant value, we substitute the x, y, and z component of the left hand of Eq. (9) to x_{proj}, y_{proj}, and z_{proj} for simplicity. The right-hand side of Eq. (9) can be expressed as Eq. (11). We use the notation of Eq. (4). Finally, by substituting the left-hand side of Eq. (9) into Eq. (10) and the right-hand side of Eq. (9) into Eq. (11), we obtain Eq. (12). Since all values in Eq. (12) except for $\sin\gamma_i$ and $\cos\gamma_i$ are constant, *we can fully determine the value of* γ_i. ■

IV. Design of *PACMAN*

Building on the derived model, we propose *PACMAN*, a method that utilizes observational data to estimate the base station's polarization and subsequently determine the optimal antenna angle for the drone. This approach enables the drone to dynamically adjust its antenna angle γ, maximizing signal alignment with the base station's polarization and thereby enhancing communication quality.

In real-world applications, several factors – such as the accuracy and granularity of motor control or environmental conditions like wind – introduce measurement errors when aligning the antenna. Recognizing this, *PACMAN* incorporates these potential inaccuracies into its alignment model. Ideally, if there were no angular error, only two measurement points P_{u_1} and P_{u_2} would suffice to determine the base station's polarization k_b, and consequently, the optimal antenna angle $f(P_u)$ at any given location.

However, due to unavoidable angular deviations, the optimal alignment angle γ at a given drone position P_u is represented as a range, $\gamma_{\min} < \gamma < \gamma_{\max}$, where the difference $\gamma_{\max} - \gamma_{\min}$ reflects the expected measurement error. For instance, if our

$$P_{S_{b,u_i}}(\hat{k_b}) = \begin{pmatrix} \sin\hat{\theta}_b \cos\hat{\phi}_b \\ \sin\hat{\theta}_b \sin\hat{\phi}_b \\ \cos\hat{\theta}_b \end{pmatrix} - \frac{X_i \sin\hat{\theta}_b \cos\hat{\phi}_b + Y_i \sin\hat{\theta}_b \sin\hat{\phi}_b + Z_i \cos\hat{\theta}_b}{X_i^2 + Y_i^2 + Z_i^2} \begin{pmatrix} X_i \\ Y_i \\ Z_i \end{pmatrix} \tag{10}$$

$$P_{S_{b,u_i}}(k_{u_i}) = \begin{pmatrix} -\sin\gamma_i \sin\alpha_i - \cos\gamma_i \sin\beta_i \cos\alpha_i \\ \sin\gamma_i \cos\alpha_i - \cos\gamma_i \sin\beta_i \sin\alpha_i \\ \cos\gamma_i \cos\beta_i \end{pmatrix} - \frac{X_i\left(-\sin\gamma_i \sin\alpha_i - \cos\gamma_i \sin\beta_i \cos\alpha_i\right) + Y_i\left(\sin\gamma_i \cos\alpha_i - \cos\gamma_i \sin\beta_i \sin\alpha_i\right) + Z_i \cos\gamma_i \cos\beta_i}{X_i^2 + Y_i^2 + Z_i^2} \begin{pmatrix} X_i \\ Y_i \\ Z_i \end{pmatrix} \tag{11}$$

$$\begin{pmatrix} x_{\text{proj}} \\ y_{\text{proj}} \\ z_{\text{proj}} \end{pmatrix} = \begin{pmatrix} -\sin\gamma_i \sin\alpha_i - \cos\gamma_i \sin\beta_i \cos\alpha_i \\ \sin\gamma_i \cos\alpha_i - \cos\gamma_i \sin\beta_i \sin\alpha_i \\ \cos\gamma_i \cos\beta_i \end{pmatrix} - \frac{X_i\left(-\sin\gamma_i \sin\alpha_i - \cos\gamma_i \sin\beta_i \cos\alpha_i\right) + Y_i\left(\sin\gamma_i \cos\alpha_i - \cos\gamma_i \sin\beta_i \sin\alpha_i\right) + Z_i \cos\gamma_i \cos\beta_i}{X_i^2 + Y_i^2 + Z_i^2} \begin{pmatrix} X_i \\ Y_i \\ Z_i \end{pmatrix} \tag{12}$$

motor operates in 15-degree increments, we have an accuracy range of 15 degrees. [4] This means that if the optimal polarization angle is actually 52°, we would achieve the strongest signal at either 45° or 60° (or potentially at both).

Instead of representing $f(P_u)$ as a range or set of candidates, we adopt an approach that fits a single optimal $f(P_u)$ by minimizing the root mean square error (RMSE) across multiple (at least 2) samples. We search for the initial base station antenna polarization $k_b = [x_{k_b}, y_{k_b}, z_{k_b}]$ by adjusting $x_{k_b}, y_{k_b}, z_{k_b}$ from -1 to +1 in increments of ϵ[5]. Given the known position of the drone, we can determine the optimal antenna angle $f(P_u)$ for each candidate k_b based on Eqs. (5) and (7) and the expansion in §III. This approach allows *PACMAN* to calculate $f(P_u)$ that minimizes the deviation from the observed measurements, providing an estimated alignment angle that most closely matches the base station's polarization. We select the k_b candidate that results in the minimal deviation across all samples, as shown below:

$$k_b = \underset{k_b}{\operatorname{argmin}} \sum_{i=1}^{N} \left(f(P_{u_i}) - \gamma_i\right)^2 \tag{13}$$

This enables *PACMAN* to provide a single alignment angle $f(P_u)$ rather than a range, guiding the antenna orientation even at unexplored locations for optimal polarization alignment.

The accuracy difference in *PACMAN*'s RMSE method based on sample variations is illustrated in Fig. 9. This graph shows the optimal antenna alignment angle for maximizing signal strength at various drone positions relative to the base station. The x-axis represents the angular displacement of the drone from the base station's pseudo-front position (the angle the drone must align with to face the base station). Negative values indicate positions to the left of the base station's front, while positive values indicate right-side positions. The drone's antenna azimuth always faces the base station. As with the definition of k_b in §III, knowledge of the exact azimuth of the base station's antenna is not required here; this is simply a relative indicator of the drone's position.

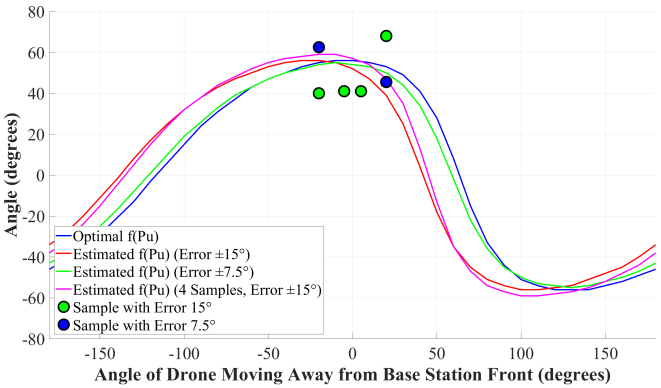

Fig. 9: Estimated optimal antenna alignment angles for different drone positions relative to the base station, using samples with varying error.

For instance, when the drone is directly in front of the base station (x-axis value 0), the optimal alignment angle is 60°. Fig. 9 illustrates estimated values of $f(P_u)$ under different sample error conditions: predictions with 15-degree error margins, 7.5-degree error margins, and four samples with 15-degree error margins, respectively. This demonstrates how *PACMAN* may perform practically. Notably, even with only two samples, our modeling approach closely identifies the optimal polarization for each position.

Our results indicate that despite limited samples with inherent inaccuracies, *PACMAN* reliably models alignment angles following the formulation in §III. In the next section, we evaluate the predicted signal strength and throughput at unexplored positions, using *PACMAN*'s recommended alignment angles derived from two exploratory samples.

PACMAN's alignment process involves two phases:

[4]Quantitatively, this quantization error is modeled as a continuous uniform distribution over the interval $[-7.5°, 7.5°]$. Consequently, the variance of the estimation error is $\sigma^2 = \frac{15^2}{12} = 18.75$, corresponding to a standard deviation of approximately $4.33°$.

[5]We use ϵ=0.05 in our proof-of-concept implementation to empirically balance computation and accuracy.

Algorithm 1 *PACMAN*: Polarization Alignment Algorithm

Require: Position of base station P_b, drone position P_u, connection information

// Phase 1: Exploration

Initialize drone enters a polarization-unknown cell
while drone rotates antenna (γ by 360°) **do**
  Measure signal strength $RSRP(\gamma)$ at each angle γ
  if $RSRP(\gamma)$ is maximized at angle $\gamma^{\max}$ **then**
    Record $\gamma^{\max}$ as a potential co-polarization angle
  end if
end while
Move drone to the next exploration position
while repeat exploration at the new position **do**
  Measure and record another $\gamma^{\max}$
end while
Calculate the base station polarization vector k_b using the two recorded $\gamma^{\max}$ values and *PACMAN* model

// Phase 2: Polarization Alignment

Calculate the optimal alignment function $f(P_u)$ based on the estimated k_b
while drone moves along the planned path **do**
  Adjust the antenna to angle $f(P_u)$ at each position
  if significant signal strength change is detected **then**
    Verify connection information
    if Base station or band changed **then**
      Return to Phase 1
    end if
  end if
end while

Phase 1: Exploration Phase. During flight, the drone performs a 360-degree scan at two initial sample points, identifying angles that maximize signal strength relative to its antenna orientation. These two samples, along with modeling differences obtained previously, enable estimation of the optimal alignment angles for subsequent positions.

Phase 2: Polarization Alignment Phase. Utilizing the predicted model from Phase 1 and the drone's planned relative positions, *PACMAN* calculates the optimal antenna alignment angle $f(P_u)$ at each point. The drone then adjusts its antenna to maintain polarization alignment dynamically. The detailed process is described in Alg. 1.

V. Evaluation

This section describes the experimental setup, presents polarization prediction and throughput gain results, and showcases a drone taxi scenario to demonstrate *PACMAN*'s real-world benefits.

A. Experiment Setup

We conduct field measurements to validate *PACMAN* using a real drone[6]. For this, we utilize the Aquila2 drone from Argosdyne, and secure the measurement equipment to the drone battery with velcro attachments (Fig. 10).

Our measurement setup consists of a Raspberry Pi 4 powered by a portable battery, two MG995 servo motors, and a directional, linearly polarized commercial off-the-shelf (COTS) antenna (oriented for horizontal polarization). The two servo motors enable 360-degree rotation of the antenna, with each motor aligned along a common rotational axis extending to the antenna. RF-isolated cables connect the antenna to the system to minimize interference. The motors operate at a speed of 0.13 seconds per 60° rotation, leading to a worst-case latency of 0.39 seconds. To ensure precise measurements while mitigating minor effects such as wind-induced shaking or slight variations in motor precision, we rotate the antenna in 15-degree increments. This setup results in 24 distinct measurement angles, ranging from 0 to 345 degrees. This configuration remains consistent across all experiments presented in this paper.

The antenna is connected to an LTE modem which provides Internet connectivity to the Raspberry Pi. We employ the EC25-EUX LTE modem, with a USIM card from a local ISP. The modem is connected to the Raspberry Pi via USB, enabling communication with the current base station through AT commands and a minicom environment. Pictures of the experimental setup can be seen in Fig. 10. The Raspberry Pi is remotely controlled via reverse SSH from the authors' computer in the lab[7].

We obtain the ground truth position of the base station from the ISP, and visited the site in-person to confirm the antenna placement. We precisely measure the position and height of the base station using a laser rangefinder. While we operate in a legally approved flight zone near the base station, in some cases, the signal can be so strong that it can be received even without an antenna. Signals leaking through non-antenna pathways disrupt accurate measurement of polarization. To address this issue and ensure precise measurements of polarization effects, we EMI-shielded the modem with copper foil tape, ensuring that no significant leakage signals are detected without an antenna. To validate the effectiveness of this shielding, we performed a pre-flight connectivity check. We confirmed that the modem immediately loses its cellular connection whenever the external antenna is disconnected, thereby verifying that signal leakage through the chassis is negligible.

Additionally, we account for the potential variation in antenna performance across different frequency bands, which could introduce noise into the polarization information. To mitigate this, we configure the experiment to use a single LTE band (i.e., LTE band 3 at 1.8 GHz) throughout the tests. Additionally, since the EC25-EUX modem does not support carrier aggregation, interference from other bands is inherently eliminated, ensuring accurate and reliable measurements. Furthermore, we monitor the connected E-UTRAN Cell ID (ECI) during the experiments to confirm that no handover occurred to another base station. Lastly, the drone operates at a speed of 5 m/s.

We conduct experiments around two distinct base stations, as shown in Fig. 11. For each base station, we define an initial reference position, position 0, where the drone faces the approximate pseudo-front of the base station. Relative positions

[6]The authors adhered to local regulations, flying within an altitude of 150 meters with registered drones only by licensed users only.

[7]The code to simultaneously control both motors and measure signal strength will be made publicly available upon acceptance of this paper.

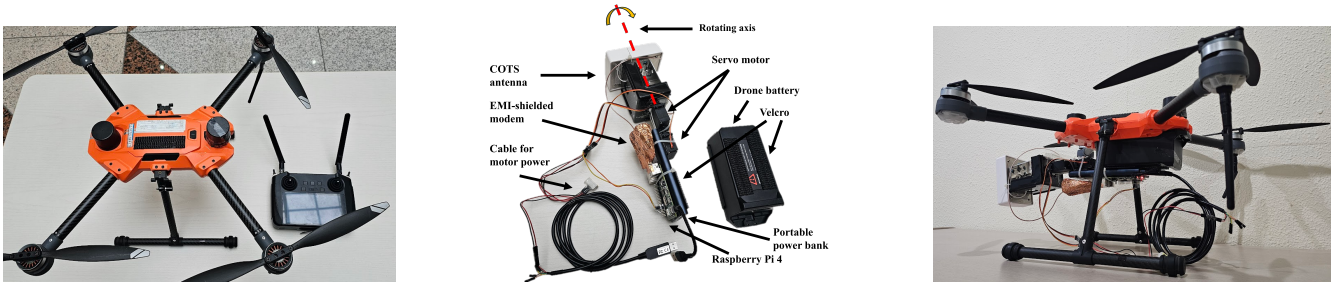

(a) Drone and Controller **(b)** Experimental Equipment and Battery **(c)** Integrated System Setup

Fig. 10: Overview of experiment setup: the drone, measurement equipment, and the integrated system

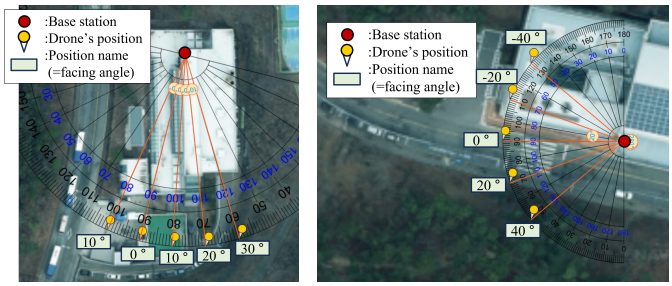

(a) Experimental Location 1 **(b)** Experimental Location 2

Fig. 11: Aerial images of the two experimental locations used for evaluating *PACMAN* performance.

are named based on the drone's facing angle with respect to this baseline. At each location, positions are carefully selected to avoid handovers and physical obstructions such as buildings or trees. At location 1, we perform two 360-degree scans at -10° and 0°, allowing us to predict optimal polarization angles for positions 10°, 20°, and 30°. The base station is positioned at an altitude of 17 meters, and the drone operates at 50 meters. At location 2, we expand the range, scanning at -40° and -20°, and estimating the best alignment angles for 0°, 20°, and 40°. Here, the base station is at 16 meters, and the drone flies 20 meters above it.

B. Finding the Best Polarization Angle

Fig. 12 presents our primary results. Following *PACMAN*, the drone initially conducts a 360-degree exploration at location 1, position -10. From this exploration, the antenna polarization angle that maximized signal strength is identified as -15°[8]. The drone then moves to the next position, position 0, where it performs another 360-degree exploration and determines the optimal antenna polarization angle to be -30 degrees.

Using the measurements from these two positions, the base station polarization vector k_b is estimated based on our model and Alg. 1. The derived base station polarization is k_b = [0.45, -0.15, 0.5]. With this polarization vector, *PACMAN* predicts the optimal antenna polarization angles for untested positions. Specifically, at position 10, the angle is estimated to be -39°; at position 20°, -45°; and at position 30°, -48°.

Subsequently, these locations are examined to verify whether the predicted angles indeed results in the strongest signal strength. As illustrated in our results, *PACMAN* successfully identifies the optimal alignment within a 15-degree margin of error in most test locations. Detailed signal strength results are summarized in Table II.

Table II presents three types of angles along with their corresponding RSRP values: (1) The optimal angle calculated by *PACMAN* ("Angle by *PACMAN*"), (2) the closest angle achievable based on the motor's rotation settings ("Selected Angle"), and (3) the angle that yields the maximum signal strength at the given position ("Best Angle"). For example, at location 1, *PACMAN* calculates angles of -39°, -45°, and -48° for positions 10, 20, and 30. However, due to the motor's 15° interval granularity, the closest achievable angles for all three positions are -45°. As summarized in the table, the selected angles successfully find the maximum signal strength in all cases. Furthermore, analyzing the difference between the best and worst RSRP (i.e., Cross-Polar Discrimination, XPD), we observe values ranging from 3.3 dB to 17.7 dB depending on the position. This significant XPD confirms that polarization mismatch can cause severe signal degradation, further justifying the need for precise alignment. These findings demonstrate that *PACMAN* can effectively achieve optimal polarization alignment.

C. Results with Different Base Stations

We extend our experiments to a new base station to verify that *PACMAN*'s model can be generalized and is not limited to a single base station. As described in §V-A and shown in Fig. 11b, the second experimental location provides a larger exploration area without obstacles. This allows us to conduct measurements at positions 40 and 20 while increasing the exploration and prediction ranges, both set at 20-degree intervals.

As shown in Fig. 13, the predicted angles align closely with the actual measurements, demonstrating the reliability of *PACMAN* in handling wider exploration and prediction ranges. A noteworthy observation is that while there are differences between the recommended angles at positions -40 and -20 and the actual angles obtained from exploration, the resulting signal strength varies only minimally. The detailed signal

[8]The drone's antenna is controlled by a motor, and the relationship between the motor control angle (γ_{motor}) and the antenna polarization angle (γ_{antenna}) is given by the equation: $360 + \gamma_{\text{antenna}} - 90 = \gamma_{\text{motor}} \pmod{180}$. For instance, if γ_{motor} = 255, then γ_{antenna} = -15.

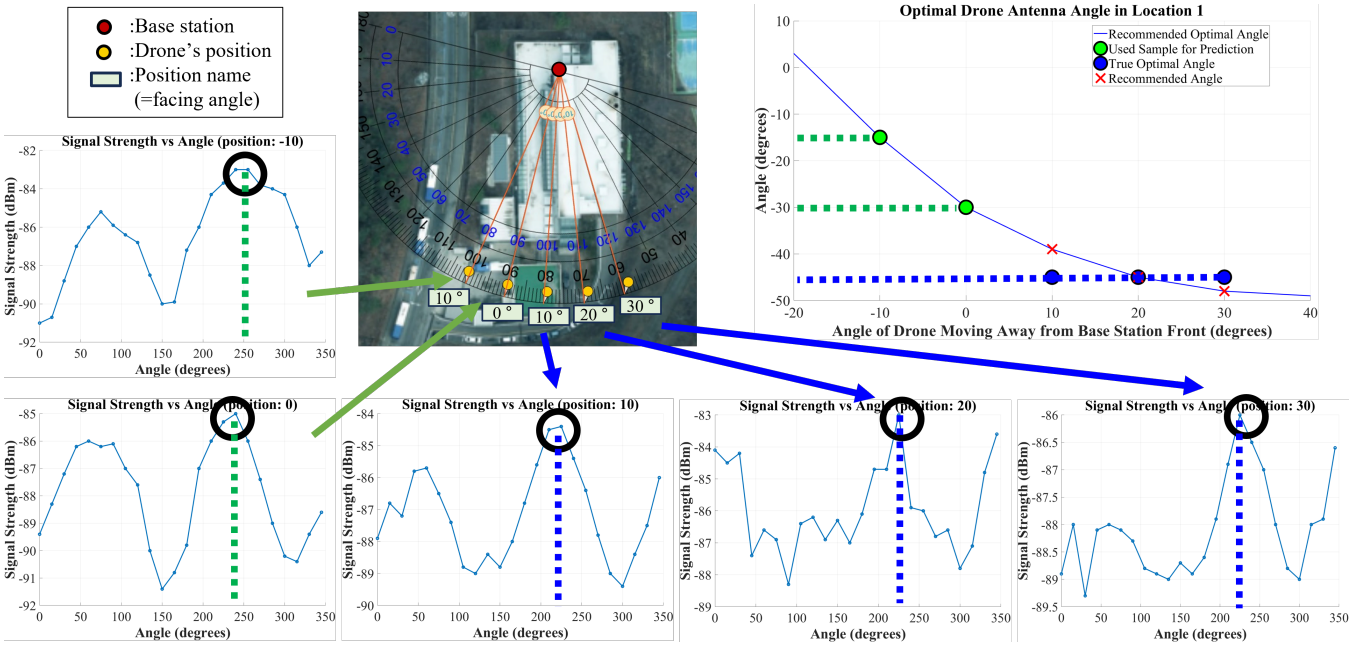

Fig. 12: Representative results for finding the best polarization angle (Location 1). Based on our analytical model and observations at 0 and -10°, *PACMAN* finds the best polarization angles at each of 10, 20, and 30° positions.

TABLE II: Comparison of polarization angles and RSRP at different angle positions for the two locations.

Location	Position	Angle selected by *PACMAN* (°)	Best angle (°)	RSRP of *PACMAN* (dBm)	Best RSRP (dBm)	Worst RSRP (dBm)	Deviation(dBm) from Best (Worst) RSRP
1	10	-39 (-45)	-45	-84.4	-84.4	-89.4	0 (+5.0)
	20	-45 (-45)	-45	-84.9	-84.9	-89.0	0 (+4.1)
	30	-48 (-45)	-45	-86.0	-86.0	-89.3	0 (+3.3)
2	0	-79 (-75)	-75	-86.4	-86.4	-104.1	0 (+17.7)
	20	-91 (-90)	-105	-87.0	-85.7	-91.9	-1.3 (+4.9)
	40	-101 (-105)	-120	-91.7	-91.0	-93.3	-0.7 (+1.6)

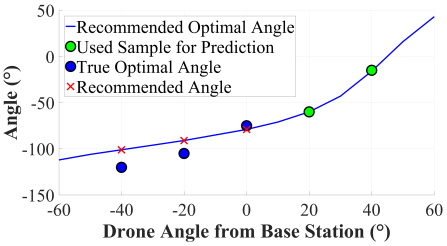

Fig. 13: Comparison of *PACMAN*'s recommended (estimated optimal) angles and the actual measured best angles at location 2.

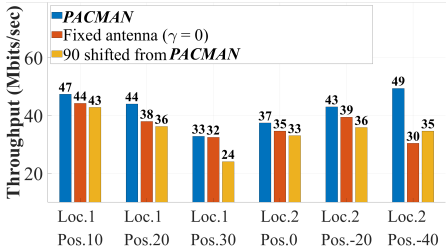

Fig. 14: TCP throughput comparison across different antenna polarization angles at two distinct locations.

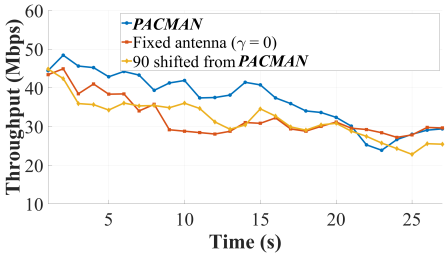

Fig. 15: Throughput during flights with same trajectory but different antenna angle configurations.

strength results are summarized in Table II. Similar results are observed as location 2. Even with slight deviations in the selected angles, the difference from the maximum achievable RSRP is only between 0.7 dBm and 1.3 dBm. These findings confirm *PACMAN*'s robustness and applicability to other base stations.

D. TCP Throughput Performance

At each untested position within the experiment sites, *PACMAN* calculates the optimal antenna angle, and we configure the antenna to the closest achievable angle based on the system's 15° resolution. We then compare the throughput under three different antenna configurations: (a) the angle recommended by *PACMAN*, (b) an angle offset by 90 degrees from the *PACMAN* recommendation (cross-pole to *PACMAN*), and (c) a fixed antenna angle of $\gamma = 0$ with no rotation.

Acknowledging that throughput can vary with time, network load, and other macro factors, we design our experiment to mitigate these influences. Specifically, we setup the iPerf server on a Gigabit Amazon server to minimize server traffic effects, and all measurements are conducted at consistent times to minimize the potential variations due to user load on the network. During a single flight, the drone hovers steadily at each position without landing, rotating only the antenna to

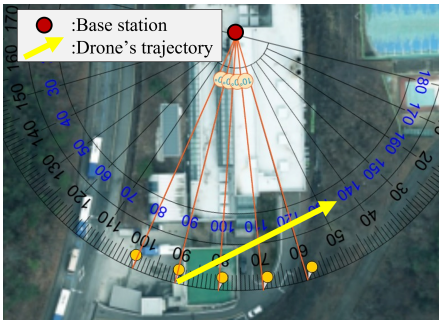

Fig. 16: Drone trajectory at the experiment site.

measure throughput for each angle. We record the average throughput over a 25-second interval for each configuration.

To ensure that the TCP congestion window has sufficient time to converge, we allow a brief pause after adjusting the antenna angle before starting throughput measurements. The entire process of sampling the three antenna configurations (i.e., *PACMAN*, fixed $\gamma = 0$, and 90° from *PACMAN*), including motor rotation, convergence time, and averaging, is completed within 3 minutes at each location. This duration is short enough to minimize the impact of environmental variations on throughput.

Fig. 14 summarizes the results of our TCP throughput experiments. For all untested locations, we achieve maximum throughput when adjusting the antenna angle to the optimal orientation recommended by *PACMAN*. The findings indicate that *PACMAN* achieves an average throughput improvement of 20.7% across six locations, with a maximum observed improvement of up to 67%.

E. Continuous Flight Experiment

Finally, we extend our evaluation to continuous flight scenarios. At the experimental site location 1, we define an arbitrary flight trajectory where the drone does not directly face the base station. Since we have already explored the polarization at this location during prior experiments, we omit Phase 1 of the exploration process. Instead, we immediately calculate the optimal antenna angles along the predefined trajectory using *PACMAN* and adjust the antenna alignment accordingly to measure throughput. Our trajectory is shown in Fig. 16.

As in the previous evaluation, we compare three configurations: (1) flying with the antenna fixed at $\gamma = 0$, (2) flying while rotating the antenna according to *PACMAN*, and (3) flying with the antenna aligned to a cross-polarization angle relative to *PACMAN*. For each antenna setting, we repeat the experiment three times and take the average throughput for comparison. The results are shown in Fig. 15.

As observed in the plot, *PACMAN* consistently demonstrates superior throughput performance throughout the drone's flight path. These findings substantiate the practical effectiveness of *PACMAN* in achieving improved throughput under realistic operational conditions.

F. Complexity and Overhead Analysis

PACMAN introduces minimal delay beyond the initial calibration. The two 360-degree scans required to build the polarization model for each base station are performed only once, taking 14.1 seconds. Afterward, computing the optimal polarization angle for a given drone position takes only 13 ms. This suggests that the computation overhead is negligible in practice. With a motor rotation speed of 0.13 sec per 60°, even a worst-case 180-degree adjustment completes within 0.4 sec. These results confirm that after calibration, *PACMAN* enables real-time dynamic polarization alignment, ensuring seamless adaptation to UAV movement.

The additional power consumption introduced by *PACMAN* is negligible. In our prototype, the UAV's total power draw during operation is approximately 415.5 W, while the Raspberry Pi and two MG995 servo motors consume only 23 W during active adjustments and 2.82 W in idle mode. Given that UAVs typically use large propulsion motors, this slight power overhead has minimal impact on flight endurance and energy efficiency.

Furthermore, the Raspberry Pi and the two servo motors are lightweight components. Their combined mass is therefore considered negligible when compared to the total operational weight of typical UAVs. Finally, *PACMAN* incurs zero *spectrum overhead* as it utilizes existing always-on reference signals (e.g., RSRP) without requiring additional pilot signals or bandwidth allocation.

VI. Discussion and Future Work

Due to equipment limitations, we could not implement MIMO configurations in our tests. However, transitioning to MIMO would not change our methodology but likely improve accuracy and precision by enabling more robust alignment. Furthermore, in ultra-dense network scenarios such as 5G and 6G, ensuring connection to the intended serving cell is crucial. As demonstrated in our experiments, monitoring the Cell ID ensures that polarization alignment is performed against the specific target base station. Since aerial users typically maintain Line-of-Sight conditions, this target-locking approach remains effective even when surrounded by dense ground infrastructure. Moreover, by mitigating polarization mismatch, *PACMAN* boosts the received signal strength, which helps stabilize the connection to the serving cell. This increased signal margin reduces the risk of frequent reconfigurations, or the ping-pong effect, often caused by signal degradation. Future work includes extending *PACMAN* to MIMO-capable UAV modems and evaluating applicability to 5G NR / mmWave deployments.

Another practical challenge is that the base station's exact polarization angle is internal information that is typically unknown. To address this, we empirically determine the strongest signal strength through comprehensive 360-degree scans, establishing a baseline for optimal alignment. From the UAV's perspective, this is more valuable than knowing the base station's actual antenna orientation, which may also be affected by ground reflections. Our evaluation confirms that *PACMAN*'s recommended angles closely align with these

empirical optima, demonstrating the robustness and reliability of our method.

We have made our collected data and measurement details (e.g., locations, base station information) public[9] to ensure transparency and reproducibility. We expect this dataset to support further research, refine UAV communication protocols, and enhance polarization alignment strategies for various UAV applications.

VII. Conclusion

This work highlighted the critical role of polarization alignment in aerial communication for UAV applications using commercial cellular networks. Based on real measurements and mathematical modeling, we developed *PACMAN*, a method that enables drones to dynamically identify and match the dominant polarization of base stations. *PACMAN* effectively identifies the optimal antenna angles at newly visited positions, and achieves near-maximum signal strength even when the angle deviates slightly with the maximum observed error being only 1.2 dBm. Real flight experiments with self-rotating antenna demonstrated throughput improvements of 20.7% on average (with a maximum of 67%), showcasing *PACMAN*'s practical benefits in aerial communication scenarios. Unlike prior research that relies on simulations or lab environments, our work demonstrates the practical effectiveness of precise polarization alignment in maximizing throughput while enhancing signal reliability and communication efficiency for robust cellular-based aerial network applications.

References

[1] Y. Yang, X. Xiong, and Y. Yan, "UAV Formation Trajectory Planning Algorithms: A Review," *Drones*, vol. 7, no. 1, 2023. [Online]. Available: https://www.mdpi.com/2504-446X/7/1/62

[2] Z. Xiaoning, "Analysis of military application of UAV swarm technology," in *3rd International Conference on Unmanned Systems (ICUS)*, 2020, pp. 1200–1204.

[3] D. Kim, J. Paek, and S. Bahk, "Lucid: LiDAR-based UAV Classification and Detection for Airspace Surveillance," in *The 46th IEEE International Conference on Distributed Computing Systems Communications (ICDCS 2026)*. IEEE, June 2026.

[4] R. I. Mukhamediev, K. Yakunin, M. Aubakirov, I. Assanov, Y. Kuchin, A. Symagulov, V. Levashenko, E. Zaitseva, D. Sokolov, and Y. Amirgaliyev, "Coverage Path Planning Optimization of Heterogeneous UAVs Group for Precision Agriculture," *IEEE Access*, vol. 11, pp. 5789–5803, 2023.

[5] J. Bae, H. Lee, and H. Lee, "A Study on Communication Technologies for Urban Air Mobility," in *13th International Conference on Information and Communication Technology Convergence*, 2022, pp. 2235–2240.

[6] Y. Gu, M. Zhou, S. Fu, and Y. Wan, "Airborne WiFi networks through directional antennae: An experimental study," in *IEEE Wireless Communications and Networking Conference*, 2015, pp. 1314–1319.

[7] C.-m. Cheng, P.-h. Hsiao, H. T. Kung, and D. Vlah, "Performance Measurement of 802.11a Wireless Links from UAV to Ground Nodes with Various Antenna Orientations," in *Proceedings of 15th International Conference on Computer Communications and Networks*, 2006, pp. 303–308.

[8] M. Asadpour, B. Van den Bergh, D. Giustiniano, K. A. Hummel, S. Pollin, and B. Plattner, "Micro aerial vehicle networks: an experimental analysis of challenges and opportunities," *IEEE Communications Magazine*, vol. 52, no. 7, pp. 141–149, 2014.

[9] D. Ryoo, Y. Yoo, J. Paek, and S. Bahk, "NOVA: Navigation Optimization via UWB-Assisted Iterative Path Planning for UAV Delivery," in *Proceedings of The IEEE International Conference on Computer Communications*. IEEE, May 2026.

[9] https://github.com/lowbyyj/polarization-alignment-TVT-public

[10] H. Wang, S. Chen, M. Ai, and H. Xu, "Localized Mobility Management for 5G Ultra Dense Network," *IEEE Transactions on Vehicular Technology*, vol. 66, no. 9, pp. 8535–8552, 2017.

[11] J. Su and F. Zheng, "Base Station Association and Handover for Cellular-Connected Multi-Antenna UAVs," in *IEEE International Black Sea Conference on Communications and Networking (BlackSeaCom)*, 2024, pp. 48–53.

[12] B. Van Der Bergh, A. Chiumento, and S. Pollin, "LTE in the sky: trading off propagation benefits with interference costs for aerial nodes," *IEEE Communications Magazine*, vol. 54, no. 5, pp. 44–50, 2016.

[13] M. Ozpolat, S. Al-Rubaye, A. Williamson, and A. Tsourdos, "Integration of Unmanned Aerial Vehicles and LTE: A Scenario-Dependent Analysis," in *International Conference on Connected Vehicle and Expo (ICCVE)*, 2022, pp. 1–6.

[14] Z. Wang and J. Zheng, "Performance Modeling and Analysis of Base Station Cooperation for Cellular-Connected UAV Networks," *IEEE Transactions on Vehicular Technology*, vol. 71, no. 2, pp. 1807–1819, 2022.

[15] P. Kyritsi, D. Cox, R. Valenzuela, and P. Wolniansky, "Effect of antenna polarization on the capacity of a multiple element system in an indoor environment," *IEEE Journal on Selected Areas in Communications*, vol. 20, no. 6, pp. 1227–1239, 2002.

[16] K.-S. Kim, J.-S. Yoo, J.-W. Kim, S. Kim, J.-W. Yu, and H. L. Lee, "All-Around Beam Switched Antenna With Dual Polarization for Drone Communications," *IEEE Transactions on Antennas and Propagation*, vol. 68, no. 6, pp. 4930–4934, 2020.

[17] B. Lindmark and M. Nilsson, "Polarization diversity gain and base station antenna characteristics," in *IEEE 49th Vehicular Technology Conference*, vol. 1, 1999, pp. 590–595 vol.1.

[18] S. Kozono, T. Tsuruhara, and M. Sakamoto, "Base station polarization diversity reception for mobile radio," *IEEE Transactions on Vehicular Technology*, vol. 33, no. 4, pp. 301–306, 1984.

[19] L. Dong, H. Choo, R. Heath, and H. Ling, "Simulation of MIMO channel capacity with antenna polarization diversity," *IEEE Transactions on Wireless Communications*, vol. 4, no. 4, pp. 1869–1873, 2005.

[20] P.-Y. Qin, Y. J. Guo, and C.-H. Liang, "Effect of Antenna Polarization Diversity on MIMO System Capacity," *IEEE Antennas and Wireless Propagation Letters*, vol. 9, pp. 1092–1095, 2010.

[21] B. Wang, C. Liao, and C.-H. Du, "A Low-Profile Broadband Dual-Polarized Base Station Antenna Array With Well-Suppressed Cross-Polarization," *IEEE Transactions on Antennas and Propagation*, vol. 69, no. 12, pp. 8354–8365, 2021.

[22] X. Quan and R. Li, "A Broadband Dual-Polarized Omnidirectional Antenna for Base Stations," *IEEE Transactions on Antennas and Propagation*, vol. 61, no. 2, pp. 943–947, 2013.

[23] B. Cheng and Z. Du, "Dual Polarization MIMO Antenna for 5G Mobile Phone Applications," *IEEE Transactions on Antennas and Propagation*, vol. 69, no. 7, pp. 4160–4165, 2021.

[24] Y. Zhu and C. Deng, "Millimeter-Wave Dual-Polarized Multibeam End-fire Antenna Array With a Small Ground Clearance," *IEEE Transactions on Antennas and Propagation*, vol. 70, no. 1, pp. 756–761, 2022.

[25] D.-C. Chang and M.-C. Huang, "Multiple-polarization microstrip reflectarray antenna with high efficiency and low cross-polarization," *IEEE Transactions on Antennas and Propagation*, vol. 43, no. 8, pp. 829–834, 1995.

[26] J. Pokorny, A. Ometov, P. Pascual, C. Baquero, P. Masek, A. Pyattaev, A. Garcia, C. Castillo, S. Andreev, J. Hosek, and Y. Koucheryavy, "Concept design and performance evaluation of UAV-based backhaul link with antenna steering," *Journal of Communications and Networks*, vol. 20, no. 5, pp. 473–483, 2018.

[27] W. Wang, Z. Fei, J. Guo, S. Durrani, and H. Yanikomeroglu, "Outage Performance of Multitier UAV Communication With Random Beam Misalignment," *IEEE Internet of Things Journal*, vol. 11, no. 3, pp. 4163–4178, 2024.

[28] M. T. Dabiri, M. Hasna, and W. Saad, "Downlink Interference Analysis of UAV-Based mmWave Fronthaul for Small Cell Networks," *IEEE Transactions on Vehicular Technology*, vol. 72, no. 5, pp. 5560–5575, 2023.

[29] J. Kim, J. Lee, and I. Lee, "Antenna Tracking Techniques for Long Range Air-to-Ground Communication Systems Using a Monopulse Method," *IEEE Access*, vol. 8, pp. 166 442–166 449, 2020.

[30] F. Wen, J. Shi, G. Gui, H. Gacanin, and O. A. Dobre, "3-D Positioning Method for Anonymous UAV Based on Bistatic Polarized MIMO Radar," *IEEE Internet of Things Journal*, vol. 10, no. 1, pp. 815–827, 2023.

[31] M. Badi, J. Wensowitch, D. Rajan, and J. Camp, "Experimental Evaluation of Antenna Polarization and Elevation Effects on Drone Communications," in *Proceedings of the 22nd International ACM Conference on Modeling, Analysis and Simulation of Wireless and Mobile Systems (MSWIM '19)*, 2019, p. 211–220.
[32] C. Ge, R. Zhang, D. Zhai, Y. Jiang, and B. Li, "UAV-Correlated MIMO Channels: 3-D Geometrical-Based Polarized Model and Capacity Analysis," *IEEE Internet of Things Journal*, vol. 10, no. 2, pp. 1446–1460, 2023.
[33] ITU-R, "Passive and active antenna systems for base stations of IMT systems," International Telecommunication Union (ITU), Tech. Rep. M.2334-0, November 2014, report ITU-R M.2334-0. [Online]. Available: https://www.itu.int/dms_pub/itu-r/opb/rep/R-REP-M.2334-2014-PDF-E.pdf
[34] Data Alliance, "45-Degree Slant Antenna Polarization Overcomes Interference and Issue w/ Dual-Polarization," https://www.data-alliance.net/blog/45degree-slant-antenna-polarization-overcomes-interference-and-issue-w-dualpolarization/.

Yongjae Yoo received his Ph.D. degree from the School of Electrical and Computer Engineering, Seoul National University, Seoul, Republic of Korea, in 2025. He received a B.S. degree in Electrical and Computer Engineering from the same university in 2019. He is now with Samsung Electronics, focusing on signal processing application system design. His research focuses on enhancing wireless networks and IoT device through advanced software solutions, real-world cellular network measurements with drones, and applying machine learning to streamline these systems.

Seungmin Choi is pursuing a B.S. degree in Electrical and Computer Engineering(ECE) at Seoul National University (SNU), Seoul, Republic of Korea. His research interests include machine learning for communications, PHY/MAC layer optimization, and signal processing for next generation networks.

Jeongyeup Paek is a tenured professor at the Department of Computer Science and Engineering, Chung-Ang University, Seoul, Republic of Korea. He received his B.S. degree from Seoul National University in 2003 and his M.S. degree from University of Southern California (USC) in 2005, both in Electrical Engineering. He then received his Ph.D. degree in Computer Science from USC in 2010. He worked at Deutsche Telekom Inc. R&D Labs USA as a research intern in 2010, and then joined Cisco Systems Inc. in 2011 where he was a Technical Leader in the Internet of Things Group. In 2014, he was with the Hongik University, Department of Computer Information Communication as an assistant professor.

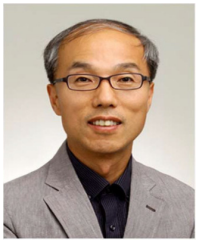

Saewoong Bahk received the B.S. and M.S. degrees in electrical engineering from Seoul National University (SNU), in 1984 and 1986, respectively, and the Ph.D. degree from the University of Pennsylvania, in 1991. He was with AT&T Bell Laboratories as a Member of Technical Staff, from 1991 to 1994, where he had worked on network management. From 2009 to 2011, he served as the Director of the Institute of New Media and Communications. He is currently a Professor at SNU. He has been leading many industrial projects on 3G/4G/5G and the IoT connectivity supported by Korean industry. He has published more than 300 technical articles and holds more than 100 patents. He is a member of the National Academy of Engineering of Korea (NAEK). He was a recipient of the KICS Haedong Scholar Award, in 2012. He was President of the Korean Institute of Communications and Information Sciences (KICS). He has been serving as Chief Information Officer (CIO) of SNU. He was General Chair of the IEEE WCNC 2020 , IEEE ICCE 2020 , and IEEE DySPAN 2018. He was Director of the Asia–Pacific Region of the IEEE ComSoc. He is an Editor of the IEEE Network Magazine and IEEE Transactions on Vehicular Technology. He was TPC Chair of the IEEE VTC-Spring 2014, and General Chair of JCCI 2015, Co-Editor-in-Chief of the Journal of Communications and Networks (JCN), and on the Editorial Board of Computer Networks Journal and the IEEE Tran. on Wireless Communications.